Fabrication of site-controlled InGaN quantum dots using reactive-ion etching

Leung Kway Lee and P.-C. Ku[*]

Department of Electrical Engineering and Computer Science, University of Michigan, 1301 Beal Ave., Ann Arbor, MI 48109, USA

* Corresponding author: e-mail peicheng@umich.edu, Phone: +1 (734) 764-7134

We adopted the simple top-down etching to fabricate site- and dimension-controlled InGaN quantum dots. Each quantum dot is disk shaped and embedded in a nanoscale pillar. Arrays of nanopillars with varying densities and nanopillar diameters were fabricated from an InGaN/GaN single quantum well using inductively-coupled plasma reactive-ion etching. Micro-photo-luminescence (μ-PL) was used to characterize the emis-sion properties of individual and ensemble of nanopillars. Strong and distinct PL signal of a single nanopillar was observed even at the room temperature. The emission was found to exhibit characteristics from a discrete en-ergy state that is homogeneously broadened. The ensem-ble of nanopillars exhibited a similar emission linewidth as the single nanopillar, indicating a well controlled quantum dot dimensions and uniformity.

1 Introduction III-nitride semiconductor quantum dots (QDs) exhibit large exciton binding energy (≥ 26 meV) [1, 2] and are ideal candidates to exploit various quantum optical phenomena at high temperatures including single-photon emission [3], strong-coupling [4, 5], indis-tinguishable photon generation [6] and one-atom lasing [7]. The practical use of the III-nitride QDs as quantum light sources often requires the addressability of a single QD. For example, strong-coupling requires the precise place-ment of a single QD at the anti-node of an optical cavity. Commonly, QDs are fabricated by the strain-induced Stranski-Krastanow (SK) growth mode which does not en-force control over the dot's site or dimension, making them difficult to be utilized on the device level. To provide site- and dimension-control to individual dots, one may apply selective area epitaxy (SAE), also known as the patterned growth [8], or the top-down approach i.e. to etch a single quantum well (SQW) into nanopillars (or nanoposts). For SAE, the site, dimension and material quality of the as-grown nanostructures are very sensitive to the growth con-dition as the growth mechanism of a patterned substrate varies significantly from an unpatterned one [8-10]. The top-down approach, on the other hand, utilizes the matured epitaxial techniques and nanolithography and serves as a more reliable method for making controlled nanostructures. Previously, the top-down approach has been used by sev-eral research groups to produce site-controlled quantum dots in III-V materials [11, 12]. For III-nitride material sys-tems, however, studies often focused on nanopillars made from multiple-quantum-wells (MQWs) [13-17]. To date, high-quality, site-controlled III-nitride quantum dots fabri-cated using the top-down approach have not been realized. In this paper, we demonstrate a viable fabrication method to produce site-controlled InGaN quantum dots exhibiting extremely good uniformity and room-temperature (RT) single-dot luminescence.

2 Sample preparation and experimental setup
The sample preparation is illustrated in Fig. 1(a). First, a 1.5-μm thick gallium nitride (GaN) template was epitaxi-ally grown on a c-plane sapphire substrate at 1050 ºC with a 25 nm low-temperature nucleation layer. After that, the template was ramped down to 760 ºC and was deposited with, firstly, a 10 nm-thick GaN layer; secondly, an InGaN layer of nominal thickness and indium composition of 3 nm and 15%, respectively; lastly, a 10 nm-thick GaN cap-ping layer. The deposition of the 10 nm low-temperature

GaN immediately before the QW layer was used to make the SQW structurally symmetric, with both QW barriers grown at 760 ºC. All epitaxial processes were carried out using a 3x2 Thomas-Swan closed-coupled showerhead MOCVD system. After epitaxial growth, arrays of nano-scale chromium (Cr) etch masks with varying diameters are patterned using electron-beam lithography (Raith 150 with MicroChem PMMA A2 resist) and the subsequent lift-off of 20-nm-thick Cr metallization (Enerjet Evaporator). Nanopillars are formed after etching the sample in an inductively coupled plasma reactive-ion etching (ICP-RIE; LAM 9400), using chlorine (Cl_2) and argon (Ar) as the etch gases. The Cr mask was removed using the chromium etchant (Cyantek CR-14) for 15 minutes. Immediately after that, 40-nm amorphous Al_2O_3 was conformally deposited by atomic layer deposition (ALD, Oxford Instruments) to provide surface passivation and to form a photonic wire structure which facilitates the out-coupling (surface-normal) of the emission from the InGaN layer [18].

Figure 1(b) shows the scanning electron micrograph (SEM) of a typical InGaN nanopillar array of period 300 nm after ICP-RIE etching. Across the sample, nanopillars with top diameters ranging from 15 to 30 nm were made. The inset of Fig. 1(b) shows a single InGaN nanopillar. Its InGaN region has a diameter of 17 nm and is located at the
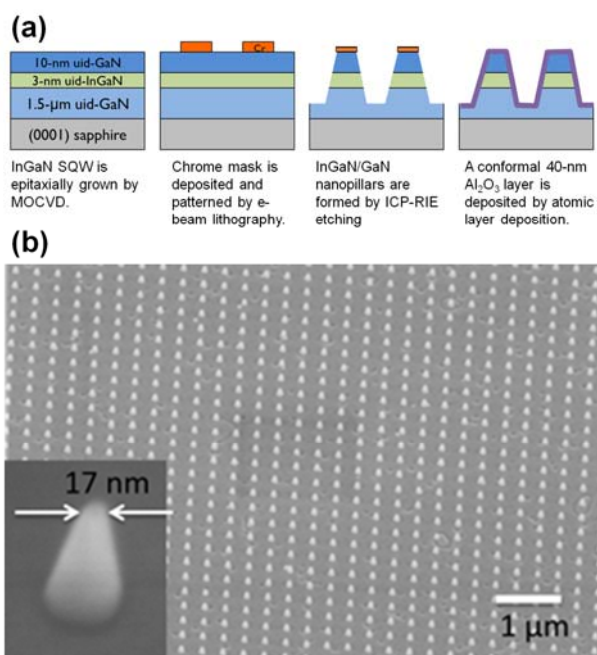

Figure 1 (a) Illustration of the process flow. (b) Scanning electron microscopy (SEM) image of nanopillars before Al_2O_3 deposition. The inset shows a standalone single pillar with a diameter of 17 nm measured at the InGaN plane.
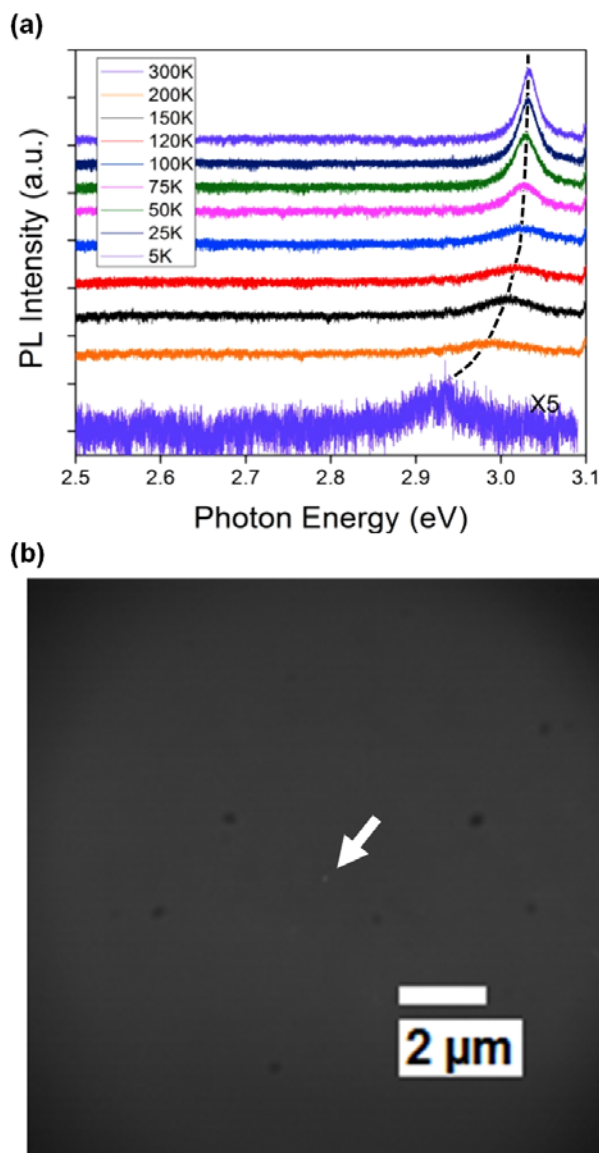

Figure 2 (a) Temperature-dependent PL of a single nanopillar. The dashed line marks the position of the emission peak and shows a trend shifting towards the lower photon energy (red-shifted). (b) Real-time CCD image of a single nanopillar at RT.

center of a 100 × 100 μm^2 area where no other InGaN structures exist. All the pillars are observed to have tapered sidewall of about 80 degree. The tapered sidewall is caused by the mask faceting effect (or the mask erosion) [19], in which the Cr nanodot etch mask shrinks in diameter due to the physical sputtering of an anisotropic ICP etching. Further evidence for the mask faceting effect comes from the observation that when the Cr nanodots are less than 15 nm, the pillars formed will have diameter larger than 30 nm and a pillar height much less than the nominal etch height of 120 nm. This implies that the smaller Cr nanodots are
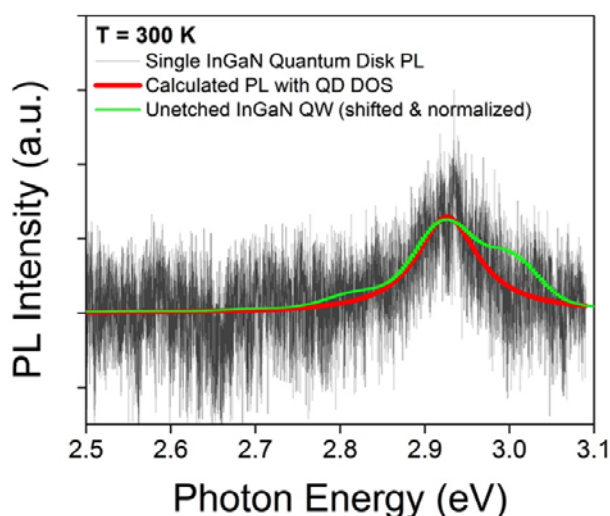
Phys. Status Solidi C **9**, No. 3–4 (2012)

611

Figure 3 Plots of RT PL of a single nanopillar, an unetched In-GaN SQW, and the calculated spontaneous emission spectrum using a 0-D density of states function. The QW PL is shifted in wavelength to make the comparison more convenient.

Figure 4 Room-temperature PL of an ensemble of 1024 nanopil-lars. Laser beam spot size was adjusted to be 10×10 μm^2 so that all 1024 nanopillars were excited.

completely sputtered away during the etching and fail to serve as etch masks, and hence the insufficient etch depth. By patterning Cr nanodots of graded diameters, the small-est top pillar diameter we can achieve while maintaining the expected etch depth was found to be 13 nm. To further shrink the nanopillar diameter, one must diminish the faceting effect by using a thicker (> 20 nm) Cr mask, in-creasing the pressure during ICP etching, and/or reducing the Ar to Cl_2 ratio to minimize the physical sputterings.

The nanopillar sample was measured using a micro-photoluminescence (μ-PL) setup equipped with a 50X ob-jective lens, responsible for both excitation and signal col-lection. The 390-nm ultrafast laser excitation was focused down to a 2-μm-diameter beam spot, giving an excitation intensity of about 5 kW/cm^2. The PL signal was dispersed by a monochromator with a 50-cm focal length and col-lected by a photomultiplier tube (PMT). The overall spec-tral resolution was 1 Å.

3 Results and discussion Temperature-dependent PL spectra of the single InGaN nanopillar shown in Fig. 1(b) inset are plotted in Fig. 2(a). First we observe that unlike in the typical InGaN quantum wells, the tempera-ture-dependent PL peak energy follows the Varshni's model $E(T)=E_0(T)-\alpha T^2/(\beta+T)$ with $\alpha = 8.54 \times 10^{-4}$ eV/K and $\beta = 550$ K instead of the S shape [20]. At 5 K, the single pillar exhibits a PL peak with a full-width-half-maximum (FWHM) linewidth of 24 meV (3.5 nm in wavelength). This FWHM linewidth is comparable to that of an SK GaN QD in Ref. [3], but is much broader than those from single SK InGaN QDs reported elsewhere [21-24] with only hun-dreds of μeV. We attributed this broad linewidth to the spectral diffusion originated from the large piezoelectric fields present in the III-nitride system [22, 23, 25, 26, 30].
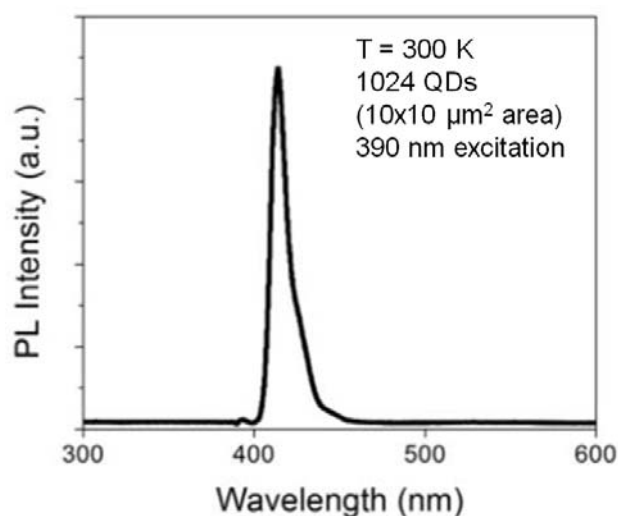
The trap centers on the etched pillar sidewalls can cause localized fluctuation of electric fields. We observe an in-creasing broadening of PL linewidth and a red shift of emission peak as the temperature rises. It is worth noting that a stand-alone single pillar exhibits distinct PL signal with a linewidth of 65 meV even at RT, which is different from other reports of self-assembled InGaN QD in which single-dot PL signal drastically diminishes and becomes difficult to detect when temperature rises above 100 K [21-24]. Figure 2(b) shows the real-time CCD image of a sin-gle nanopillar under 390-nm laser excitation at RT. The large linewidth at RT is believed to be phonon assisted. From the integrated PL intensity and assuming the radia-tive efficiency at 5 K to be 100%, the radiative efficiency of the single nanopillar was found to be 33% which was at-tributed to the low surface recombination velocity [27].

We also note that the RT PL spectrum of a single pillar is quite symmetric compared to a typical QW PL in which the asymmetric high-energy tail presents [28]. The high-energy tail originates from the integration of Fermi-Dirac distribution function of the carriers with the two-dimensional density of state and is a characteristic of QW PL [28, 29]. The RT PL signal of a single nanopillar is fit-ted with the spontaneous emission of QD as described in Ref. [29]. The result of the fitting is shown in Fig. 3. As a comparison, the PL of the unetched SQW sample is also shown (with its peak wavelength shifted for visual conven-ience). It is evident that the PL from the single InGaN nanopillar fits well with the QD curve but not the QW. We have also observed the size quantization effect, a important characteristic of the quantum dot. The blue shift from a 24-nm disk to a 16-nm disk was measured to be 60 meV and cannot be solely attributed to strain relaxation. The detailed modeling of the size quantization effect will be presented else-where. The above results strongly suggest that the

disk-shaped InGaN region possess emission characteristics closer to a QD than a QW. Finally, a more rigorous proof of the QD-like emission properties will require the measurement of photon antibunching and is currently underway.

Figure 4 shows the PL from an ensemble of InGaN nanopillars measured at RT. It is seen that the emission linewidth is 63 meV which is the same as that of the single InGaN nanopillar. This implies an extremely well-controlled nanopillar diameters and uniformity. We also observed no obvious yellow band luminescence (YBL) which is an indication of the high materials quality even after the ICP-RIE process. It may be attributed to the conformal coating of Al_2O_3 by ALD which passivates the surface. In a separate sample without the Al_2O_3 passivation, we indeed observed the formation of YBL over time.

4 Conclusion We demonstrated that the simple top-down approach by dry etching is viable to fabricate high-quality site- and dimension-controlled InGaN quantum dots from an InGaN SQW sample using reactive-ion etching. We characterized the emission properties of a single InGaN nanopillar using temperature-dependent micro-photoluminescence. Distinct PL signal was observed even at RT which agreed well with the calculated QD emission and was markedly different from the unetched QW PL. The ensemble exhibited a similar emission linewidth as the single nanopillar, indicating the extremely well-controlled nanopillar size and uniformity.

References

[1] Y. Narukawa, Y. Kawakami, S. Fujita, S. Fujita, and S. Nakamura, Phys. Rev. B **55**, R1938 (1997).

[2] W. Huang and F. Jain, J. Appl. Phys. **87**, 7354 (2000).

[3] S. Kako, C. Santori, K. Hoshino, S. Götzinger, Y. Yamamoto, and Y. Arakawa, Nature Mater. **5**, 887 (2006).

[4] G. Khitrova, H. M. Gibbs, M. Kira, S. W. Koch, and A. Scherer, Nature Phys. **2**, 81 (2006).

[5] K. Hennessy, A. Badolato, M. Winger, D. Gerace, M. Atatüre, S. Gulde, S. Fält, E. L. Hu, and A. Imamoğlu, Nature **445**, 896 (2007).

[6] C. Santori, D. Fattal, J. Vučković, G. S. Solomon, and Y. Yamamoto, Nature **419**, 594 (2002).

[7] M. Nomura, N. Kumagai, S. Iwamoto, Y. Ota, and Y. Arakawa, Nature Phys. **6**, 279 (2010).

[8] P. Chen, A. Chen, S. J. Chua, and J. N. Tan, Adv. Mater. **19**, 1707 (2007).

[9] J. Yamaguchi and K. Okamoto, Jpn. J. Appl. Phys. **32**, 1523 (1993).

[10] J. Yamaguchi, J. Ogasawara, and K. Okamoto, J. Appl. Phys. **72**, 5919 (1992).

[11] R. Steffen, Th. Koch, J. Oshinowo, F. Faller, and A. Forchel, Appl. Phys. Lett. **68**, 223 (1996).

[12] C. Schneider, T. Heindel, A.Huggenberger, P. Weinmann, C. Kristner, M. Kamp, S. Reitzenstein, S. Höfling, and A. Forchel, Appl. Phys. Lett. **94**, 111111 (2009).

[13] S. Keller, C. Schaake, N. A. Fichtenbaum, C. J. Neufeld, Y. Wu, K. McGroddy, A. David, S. P. DenBaars, C. Weisbuch, J. S. Speck, and U. K. Mishra, J. Appl. Phys. **100**, 054314 (2006).

[14] Y. He, L. Chen, Y.-K. Song, A. V. Nurmikko, S.-R. Jeon, Z. Ren, M. Gherasimova, and J. Han, Phys. Status Solidi C **2**, 2740 (2005).

[15] H.-S. Chen, D.-M. Yeh, Y.-C. Lu, C.-Y. Chen, C.-F. Huang, T.-Y. Tang, C.-C. Yang, C.-S. Wu, and C.-D. Chen, Nanotechnology **17**, 1454 (2006).

[16] V. Ramesh, A. Kikuchi, K. Kishino, M. Funato, and Y. Kawakami, J. Appl. Phys. **107**, 114303 (2010).

[17] P. Yu, C. H. Chiu, Y.-R. Wu, H. H. Yen, J. R. Chen, C. C. Kao, H.-W. Yang, H. C. Kuo, T. C. Lu, W. Y. Yeh, and S. C. Wang, Appl. Phys. Lett. **93**, 081110 (2008).

[18] J. Heinrich, A. Huggenberger, T. Heindel, S. Reitzenstein, S. Höfling, L. Worschech, and A. Forchel, Appl. Phys. Lett. **96**, 211117 (2010).

[19] M. J. Madou, Fundamentals of Microfabrication: The Science of Miniaturization, 2nd ed. (CRC Press LLC, Boca Raton, 2002), chap. 2.

[20] Y.-H. Cho, G. H. Gainer, A. J. Fischer, J. J. Song, S. Keller, U. K. Michra, and S. P. DenBaars, Appl. Phys. Lett. **73**, 1370 (1998).

[21] K. Sebald, H. Lohmeyer, J. Gutowski, T. Yamaguchi, and D. Hommel, Phys. Status Solidi B **243**, 1661 (2006).

[22] R. Seguin, S. Rodt, A. Strittmatter, L. Reißmann, T. Bartel, A. Hoffmann, D. Bimberg, E. Hahn, and D. Gerthsen, Appl. Phys. Lett. **84**, 4023 (2004).

[23] J. H. Rice, J. W. Robinson, J. D. Smith, A. Jarjour, R. A. Taylor, R. A. Oliver, G. Andrew, D. Briggs, M. J. Kappers, S. Yasin, and C. J. Humphreys, IEEE Trans. Nanotechnol. **3**, 343 (2004).

[24] H. Schömig, S. Halm, A. Forchel, G. Bacher, J. Off, and F. Scholz, Phys. Rev. Lett. **92**, 106802 (2004).

[25] J. H. Rice, J. W. Robinson, A. Jarjour, R. A. Taylor, R. A. Oliver, G. Andrew, D. Briggs, M. J. Kappers, and C. J. Humphreys, Appl. Phys. Lett. **84**, 4110 (2004).

[26] S. A. Empedocles and M. G. Bawendi, Science **278**, 2114 (1997).

[27] J. B. Schlager, K. A. Bertness, P. T. Blanchard, L. H. Robins, A. Roshko, and N. A. Sanford, J. Appl. Phys. **103**, 124309 (2008).

[28] H. Zhao, G. Liu, and N. Tansu, Appl. Phys. Lett. **97**, 131114 (2010).

[29] S. L. Chuang, Physics of Optoelectronic Devices (Wiley-Interscience, New York, 1995), pp. 157-160, 345-351.

[30] J. H. Rice, J. W. Robinson, J. H. Na, K. H. Lee, R. A. Taylor, D. P. Williams, E. P. O'Reilly, A. D. Andreev, Y. Arakawa, and S. Yasin, Nanotechnology **16**, 1477 (2005).